

Effect of Stacking Order on the Electronic State of 1T-TaS₂

Zongxiu Wu,¹ Kunliang Bu,¹ Wenhao Zhang,¹ Ying Fei,¹ Yuan Zheng,¹
Jingjing Gao,^{2,3} Xuan Luo,² Zheng Liu,⁴ Yu-Ping Sun,^{2,5,6} and Yi Yin^{1,6,*}

¹Zhejiang Province Key Laboratory of Quantum Technology and Device,
Department of Physics, Zhejiang University, Hangzhou 310027, China

²Key Laboratory of Materials Physics, Institute of Solid State Physics,
Chinese Academy of Sciences, Hefei 230031, China

³University of Science and Technology of China, Hefei 230026, China

⁴Institute for Advanced Study, Tsinghua University, Beijing 100084, China

⁵High Magnetic Field Laboratory, Chinese Academy of Sciences, Hefei 230031, China

⁶Collaborative Innovation Center of Advanced Microstructures, Nanjing University, Nanjing 210093, China

New theoretical proposals and experimental findings on transition metal dichalcogenide 1T-TaS₂ have revived interest in its possible Mott insulating state. We perform a comprehensive scanning tunneling microscopy and spectroscopy experiment on different single-step areas in pristine 1T-TaS₂. After accurately determining the relative displacement of the Star-of-David super-lattices in two layers, we find different stacking orders corresponding to different electronic states measured on the upper terrace. The center-to-center stacking corresponds to the universal large gap, while other stacking orders correspond to a reduced or suppressed gap in the electronic spectrum. Adopting a unified model, we conclude that the universal large gap is a correlation-induced Mott gap from the single-layer property. Our work provides more evidence about the surface electronic state and deepens our understanding of the Mott insulating state in 1T-TaS₂.

I. INTRODUCTION

The correlation of electrons in many cases plays a crucial role in determining special physical properties of quantum materials [1–4]. The layered transition metal dichalcogenide (TMD) 1T-TaS₂ is a long-known charge density wave (CDW) material with a rich phase diagram [5–7]. In the commensurate CDW (CCDW) phase, every 13 Ta atoms shrink into a CDW cluster called star of David (SD) and establish a $\sqrt{13} \times \sqrt{13}$ electronic reconstruction. Recently rekindled interest in 1T-TaS₂ originates from the possible Mott insulating state in the CCDW phase. The multi-folded band of SD super-lattice induces a flat band around the Fermi energy, whose narrow bandwidth pushes the low-energy physics to a strong correlation limit. The conventional view is that each SD contributes one unpaired electron forming a half-filled flat band near the Fermi level. With the relatively strong correlation of electrons, the half-filled band splits into lower and upper Hubbard bands (LHB and UHB), resulting in a Mott insulating gap [1]. The insulating state has been identified by many experiments like transport, scanning tunneling microscopy (STM), angle-resolved photoemission spectroscopy (ARPES), *etc* [7–9]. Based on this single-band Mott insulator scenario, many exotic phases like superconducting and quantum spin liquid state have been proposed and explored [10–15].

However, there remain some long-standing unsolved issues about the nature of the insulating state [16, 17]. Although the density functional theory (DFT) calculation with the onsite-U correction can reproduce a Mott gap

in a single-layer 1T-TaS₂, the calculation always yields a metallic band along the *c*-axis when the 1T-TaS₂ layers are stacked periodically, inconsistent with the experimental insulating state [18]. A further DFT calculation shows that different stacking orders can change the electronic state on the *ab*-plane but cannot gap the metallic band along the *c*-axis [19, 20]. Another group performed a more detailed DFT calculation and proved that a particular stacking order might open a gap in the whole Brillouin zone [21]. Experimentally, recent STM results revealed two typical terminals showing insulating gaps with different gap sizes [22–24]. The small-gap, large-gap, and small-gap spectra have been found on consecutive three terraces [22]. The large-gap spectrum measured on the upper terrace corresponds to an AA-stacking order, in which the SD centers in the upper and lower layers are aligned. With a unit-cell doubling model, they suggest that the large gap on this terminal is a band gap, while the small gap on a misaligned terminal is the single-layer Mott insulating gap. The high-resolution synchrotron x-ray diffraction (XRD) and ARPES measurements also found some ambiguous evidence of dimerization along the *c*-axis, and simplified the insulating state into a trivial band insulator [25, 26].

These DFT and experimental results seem to be compatible, while some fundamental questions still exist. Both results are strongly against the conventional single-band Mott scenario in 1T-TaS₂. Some DFT calculations suggested that electron correlation was not a necessary ingredient to understand the insulating state, while the STM results still claim a Mott insulating gap on the misaligned terminal. Some previous experiments show that the large gap can be effectively tuned by external parameters such as strain, doping, and intercalation [10–12, 27–31], which cannot be simply explained by the band

* yiyin@zju.edu.cn

insulator scenario. The molecular beam epitaxy (MBE)-grown single-layer TMDs $1T$ -TaS₂ and $1T$ -TaSe₂ exhibit a large insulating gap [32, 33], consistent with the most frequently observed large-gap spectrum in bulk $1T$ -TaS₂.

To address the above questions, we implement a systematic and comprehensive STM study on the stacking order and corresponding electronic state of $1T$ -TaS₂. We report accurate determination of various inter-layer alignments of SD super-lattices and the associated dI/dV spectra by exploring single-step areas of the cleaved $1T$ -TaS₂. Through multiple measurements, we find that AA-stacking order is dominant in $1T$ -TaS₂. The AC-stacking is often observed around the step edge, while the AB-stacking is only occasionally seen. The AC-AA-AC-AA stacking order can only be an occasional case near the surface, due to some randomness in stacking order. The AA-stacking is associated with a top large-gap spectrum. Besides, the top large-gap spectrum occasionally appears at different stacking orders. These observations cannot be explained by a simple inter-layer dimerization mechanism [21–26]. The large gap is therefore most possibly a single-layer feature, a correlation-driven Mott gap. For the AC- and AB-stacking orders, the top dI/dV spectra exhibit a small-gap spectrum and a metallic V-shaped spectrum, respectively. Although AA-stacking minimally affects the single-layer property, other stacking orders could perturb the Mott gap and modulate the pristine large-gap insulating state.

II. EXPERIMENT AND RESULTS

Each layer of $1T$ -TaS₂ is comprised of a triangular lattice of Ta atoms sandwiched between the top and bottom triangular lattice of S atoms. Each Ta atom is coordinated octahedrally by S atoms. In the CCDW phase, each SD cluster is formed by 13 Ta atoms, roughly classified by one central Ta atom (position A), six neighboring Ta atoms at inner-corner site (position B), and six next neighboring Ta atoms at outer-corner site (position C and C'). In our previous work [29], we found that a substrate with different thermal expansion coefficient than the sample can induce local strain and change the surface appearance. Here we glue the sample on a silica substrate, and cleave the sample at liquid nitrogen (LN₂) temperature. Most cleaved surfaces are still flat as shown in Fig. 1(b), while it is relatively easy to find a surface topography with steps as shown in Fig. 1(d). The cleaved sample is thereafter quickly transferred to the STM scan head in the cryogenic Dewar. We also perform the following STM measurement at LN₂ temperature.

The SD super-lattice is discerned in the flat surface topography [Fig. 1(b)], with each bright spot representing one SD. When the tip is sharp enough, the surface exposed S atoms can be atomically resolved within SDs [inset of Fig. 1(b)]. A typical dI/dV spectrum measured at one SD center is shown in Fig. 1(c). The two coherence peaks are well established roughly at ± 200 mV.

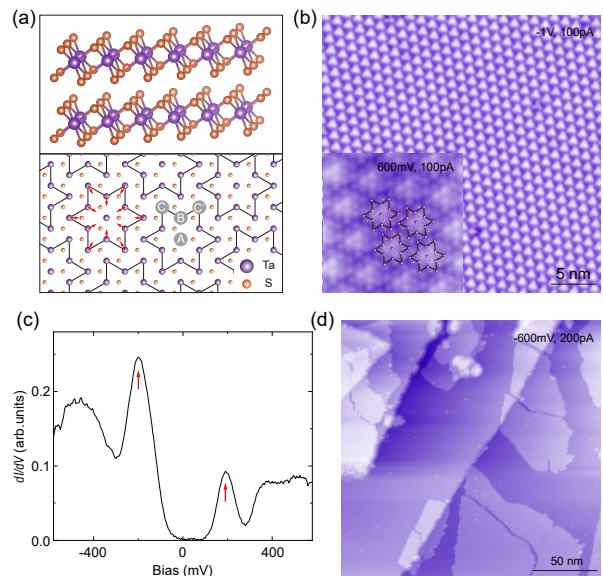


FIG. 1. Structural and electronic properties of $1T$ -TaS₂. (a) The upper panel shows the atomic structure of $1T$ -TaS₂. The lower panel is a top-view diagram, with the purple and yellow balls representing the Ta atoms and the uppermost S atoms, respectively. Ta atom positions can be divided into central, inner-corner, and outer-corner cases, which are labeled by A, B, and C (C'), respectively. The red arrow indicates the shrinking of the surrounding 12 Ta atoms toward the central Ta. (b) A typical $30 \times 30 \text{ nm}^2$ topography in a flat area. The inset displays an atomically resolved topography under the tunneling condition of $V_b = 600 \text{ mV}$, $I = 100 \text{ pA}$. (c) The typical insulating dI/dV spectrum of $1T$ -TaS₂. The red arrows label the upper and lower Hubbard bands. (d) A complex surface topography.

The resulting insulating gap of 400 meV has been conventionally considered as a Mott gap between the LHB and UHB. Peaks outside the Hubbard bands are associated with CDW features.

The flat single-step area renders a determination of the relative displacement of SD super-lattices in the upper and lower layers. Multiple measurements have been collected for different samples with different tips. Figure 2(a) shows the topography of the most common example of a single-step area. For both smooth top and underlying layers, the topography includes a triangular SD super-lattice and each bright spot represents one SD. Two typical dI/dV spectra measured on the lower and upper terraces are displayed in Fig. 2(b), both similar to the spectrum in Fig. 1(c). To check how the spectrum evolves, a linecut map is measured along the arrowed line in Fig. 2(a). As shown in Fig. 2(c), the linecut map of dI/dV spectrum is vertically displayed in color in the top panel, corresponding to the height profile in the bottom panel. On both the lower and upper terraces, the dI/dV spectrum shows a periodic intensity variation, and shares the similar large-gap feature except for some modulations at the step edge.

With both the upper and lower terraces exposed, we

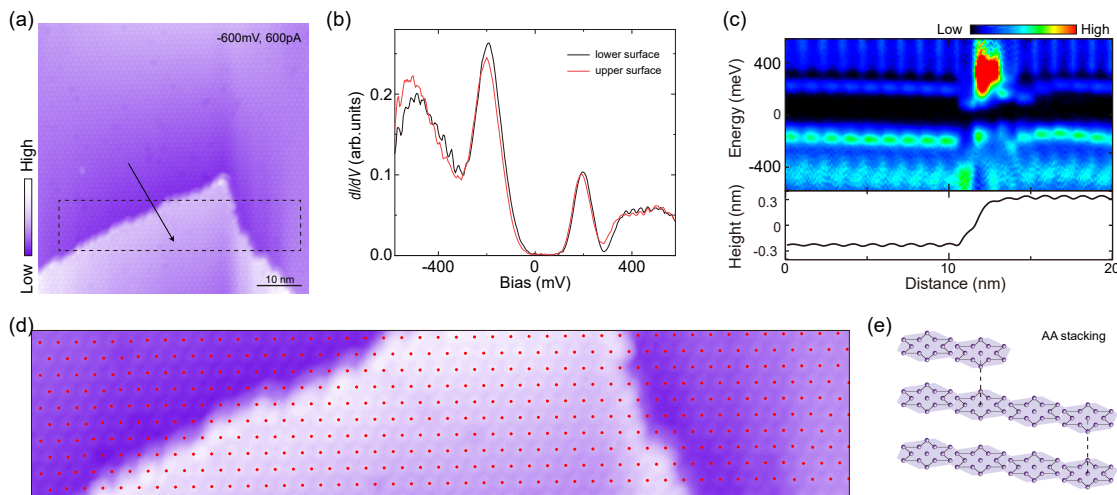


FIG. 2. AA-stacking single-step area with a top large-gap spectrum. (a) STM topography of the single-step area. (b) The red and black curves show the dI/dV spectra on the upper and lower terraces, respectively. Both spectra are similar to the typical spectrum in Fig. 1(c). (c) A series of dI/dV spectra measured along the black arrowed line in (a), with the height profile displayed in the lower panel. (d) The determination of SD super-lattice for area within the black dashed frame in (a). (e) A schematic diagram of the AA-stacking order.

analyze the relative displacement of the upper and lower super-lattices. We choose a rectangular area enclosing a top peninsula area. Around each corner, several SD centers are positioned with a peak-seeking algorithm. With anchored positions between different corners, a linear fitting leads to a SD array for the lower layer, as shown by the red dots in Fig. 2(d). The positioning accuracy can be confirmed by comparing the dot position with the SD in topography, for the exposed part of lower layer. We further observe that the red dots at the peninsula coverage area coincide with the SD centers in the upper layer. The SD centers in the upper and lower layers are aligned along the c -axis. This stacking order can be defined as the AA-stacking order [Fig. 2(e)].

In the process of collecting and analyzing data, we occasionally find some misaligned examples in which the large-gap spectrum is obtained on both the upper and lower terraces. Figure 3(a) and (b) display two topographies around different single-step areas. The SD centers are positioned on both the upper (blue dots) and lower (red dots) terraces, with red dots also linearly extended to the upper terrace. We can observe that the SD centers in the upper layer are misaligned with those in the lower layer. The stacking orders in Fig. 3(a) and (b) are determined to be AC'-stacking and AB-stacking orders, respectively. Figure 3(c) and (d) display the corresponding dI/dV spectra measured on the lower and upper terraces, respectively. They all share the similar large-gap feature in spectrum.

The large insulating gap is the most identified spectrum feature in our experiment. For all single-step areas, spectrum on the lower terrace exhibits the large-gap spectrum. For the occasional examples in Fig. 3, the upper-layer spectrum is not strongly altered in AC'- or AB-stacking conditions, with zero-bias conductance

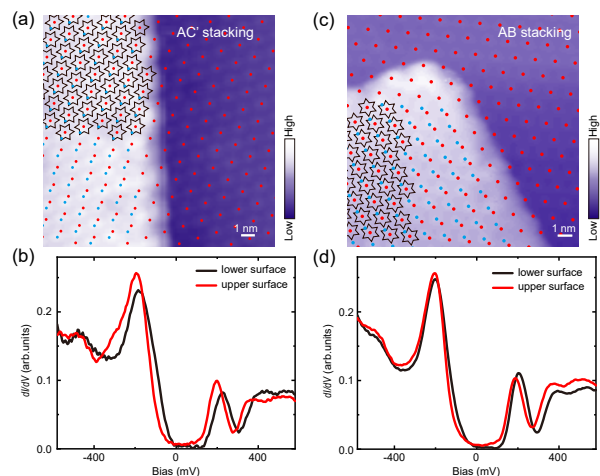


FIG. 3. Two misaligned examples on the single-step area. (a), (b) STM topography of the single-step area. The red (blue) dots label SD centers in the lower (upper) layer, showing a misaligned configuration. (c), (d) The red and black curves show the corresponding dI/dV spectra on the upper and lower terraces in (a) and (b), respectively.

slightly enhanced. We notice that the large-gap spectrum has been previously found in AC'-stacking condition in a metastable system induced by voltage pulses [34], whereas our results are all in a stable state. The consecutive two large-gap spectra on two terraces (Fig. 2), instead of the alternating large- and small-gap spectra, rule out the possibility that the large-gap spectrum originates from a unit-cell doubling of two AA-stacked layers. The consecutive two large-gap spectra in Fig. 3 further exclude the unit-cell doubling mechanism. A more reasonable model is that the large-gap spectrum reflects the

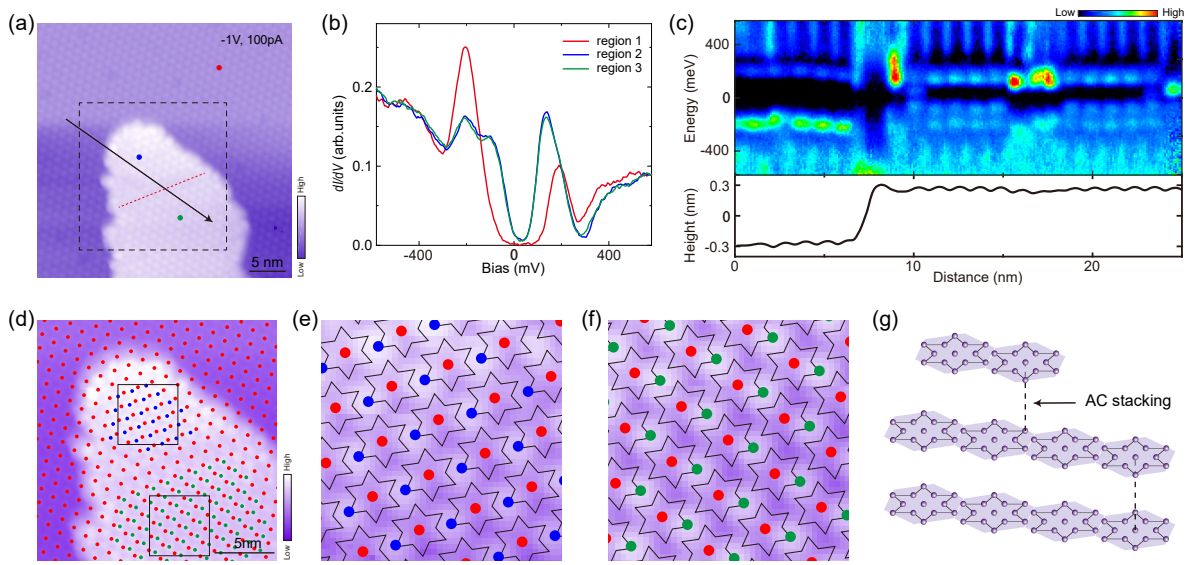


FIG. 4. AC-stacking single-step area with a top small-gap spectrum. (a) STM topography of the single-step area. The red dashed line indicates a domain wall on the top terrace. (b) Three dI/dV curves correspond to the electronic states measured at the red, blue, and green dot positions in (a), respectively. The spectrum on the lower terrace is the typical insulating spectrum, and the spectrum on both sides of the domain wall on the upper terrace is one with a smaller gap. (c) A series of dI/dV spectra measured along the black arrowed line in (a), with the height profile displayed in the lower panel. (d) The determination of SD super-lattices for area within the black dashed frame in (a). The red dots label SD centers in the lower layer, and the blue and green dots label SD centers in the area on two sides of the domain wall. (e), (f) The enlargement of the two black boxes in (d). The SD centers in the upper layer are all aligned with the SD outer-corner sites in the lower layer. (g) A schematic diagram of the AC-stacking order.

single-layer property, like that measured on the single-layer MBE grown film of $1T$ -TaS₂ [32, 33]. Then the universal large insulating gap is still a single-layer Mott insulating gap.

Besides the universal large insulating gap, other types of dI/dV spectra have been observed on the upper terrace of different single-step areas. An example of the common case is shown in Fig. 4. Figure 4(a) displays a topography with a top peninsula area. The red dashed line on the upper terrace marks a domain wall. The SD super-lattices within two domains are shifted relative to each other. At locations of three points marked in the image, the dI/dV spectra are measured on the lower terrace, and two domains on the upper terrace, respectively. As shown in Fig. 4(b), the spectrum on the lower terrace is still an insulating spectrum similar to that in Fig. 1(c). In contrast, the spectra measured within both domains on the upper terrace are different. The UHB peak is shifted to 140 mV, and the LHB splits to two peaks at -100 and -205 mV. Following we call this type of spectrum a small-gap spectrum. A linecut map is measured along the arrowed line in Fig. 4(a), with the results shown in Fig. 4(c). Together with the periodic intensity variation, the dI/dV spectrum shows a large-gap spectrum on the lower terrace and a small-gap spectrum on the upper terrace, except for some modulations at the step edge and domain wall.

To study the stacking order in Fig. 4, we position the SD centers in three regions around the peninsula area.

A SD array is extracted for the lower layer, as shown by the red dots in Fig. 4(d). The SD centers in the upper layer, labeled by blue and green dots for two domains, are observed to be not aligned with those in the lower layer. Due to the lattice symmetry in $1T$ -TaS₂, positioning of SD centers corresponds to two possible atomic arrangements, which differ with a 27.8° rotation of each SD. We further apply a specific point defect to obtain the only definite atomic lattice of the lower layer, with the method shown in Appendix A. Correspondingly, both the SD centers and the SD arrangement in the lower layer are superimposed on the enlarged topographies in Fig. 4(e) and 4(f). We can observe that the SD centers in the upper layer are aligned with different but equivalent next nearest Ta atoms in each SD in the lower layer. This stacking order is defined as the AC-stacking order [Fig. 4(g)].

The similar small insulating gap has been reported with the same stacking order in recent STM experiments [22–24]. The -100 and 140 mV peaks have been considered as the LHB and UHB of a single-layer Mott state, leaving the -205 mV peak unexplained. From the periodic intensity variation of dI/dV spectrum on the upper terrace [Fig. 4(c)], we observe that the three shifted peaks around Fermi energy (zero bias) are still evident at the SD centers, representing that they are from the Hubbard bands of central Ta orbital [28]. Since we consider the large-gap spectrum a single-layer property, the small-gap spectrum in our opinion is a perturbed and reduced Mott gap in the AC-stacking configuration. To explain

the split of LHB is still beyond our current understanding.

During the measurement of single-step areas, we find that the correspondence between stacking orders and electronic states in Fig. 2 and Fig. 4 are constantly reproducible. Another occasional case is presented in Appendix B, in which the AB-stacking order corresponds to a metallic spectrum on the upper terrace. In addition, we never observe the AA-stacking order together with a small-gap or metallic spectrum, consistent with that the AA-stacking order minimally affects the single-layer large-gap spectrum. For the case in Fig. 2, the large-gap spectrum on the upper terrace can extend all the way in from the step edge. On the contrary, the small-gap and metallic spectra on the upper terrace often exist within a certain range of the step edge, e.g. 20 nm. The AA-stacking order seems to be an energy optimal situation in bulk $1T$ -TaS₂. Sometimes the AC-stacking occurs around the step edge. Because the dI/dV measured on the lower terrace is always a large-gap spectrum, we assume that the lower terrace is also AA-stacked with the unexposed layer below, as depicted in Fig. 2(e), Fig. 4(e), and Fig. 6(f). The normal flat surface is considered to be AA-stacked with the underlying layer, resulting in a large-gap insulating spectrum.

III. CONCLUSION

We note that all the typical spectra shown in [22] are also observed in our experiment, but a key difference is that we show for AA-stacking the large-gap spectra does not necessarily change across the step. This largely rules out a successive AC-AA-AC-AA alternating stacking order in bulk $1T$ -TaS₂. In contrast to a AA dimerization scenario, the large insulating gap can actually be well compared with that observed in a MBE grown single layer TaS₂ [32]. Note that although the large-gap spectrum could reflect the single-layer property of $1T$ -TaS₂, the special slope from LHB to zero bias position may be associated with inter-layer effect along the c -axis. A most recent DFT calculation suggests that the conventional use of atomic-orbital basis could seriously mis-evaluate the electron correlation in the CDW state [35]. By adopting a generalized basis, they successfully reproduce the Mott insulating state under AA-stacking order condition in $1T$ -TaS₂, consistent with our results.

In conclusion, our experimental results show that the large insulating gap is a correlation-driven Mott gap feature of a single-layer $1T$ -TaS₂, which is nearly unperturbed under AA-stacking. The misaligned stacking orders may disturb the Mott gap to a small-gap or metallic spectrum. A possible explanation is that the misalignment weakens the CCDW amplitude, on which the Mott physics sensitively relies. Further theoretical investigations are required to clarify the subtle interplay between electron correlation, CDW and stacking order effect.

ACKNOWLEDGMENTS

This work was supported by the National Key Research and Development Program of China (Grants No. 2019YFA0308602), the Key Research and Development Program of Zhejiang Province, China (2021C01002), and the Fundamental Research Funds for the Central Universities in China. Z.L. thanks the National Nature Science Foundation of China (NSFC-11774196) and Tsinghua University Initiative Scientific Research Program. J.J.G., X.L., and Y.P.S. thank the support of the National Key Research and Development Program of China (Grants No. 2016YFA0300404), the National Nature Science Foundation of China (NSFC-11674326 and NSFC-11874357), the Joint Funds of the National Natural Science Foundation of China, and the Chinese Academy of Sciences' Large-Scale Scientific Facility (U1832141, U1932217, U2032215).

Appendix A: A Special Type of Point Defect in $1T$ -TaS₂

Figure 5 shows representative data for a particular type of defect we find in $1T$ -TaS₂. Figure 5(a) and 5(b) are two topographic images taken at the same area with bias voltage at 600 mV and -1000 mV, respectively. A three-petal shaped defect can be observed in the middle of both images, pointing in the same direction but with the three petals in Fig. 5(b) gathered closer. We notice that each SD is a triangle in the topography, with the direction of triangle in both topographies inverted. Figure 5(c) shows two dI/dV spectra measured at the center of the three-petal defect and a normal SD. Compared with the normal large-gap spectrum, the defect spectrum shows a totally suppressed UHB while the LHB is left with a raised peak at -300 mV.

Occasionally, the atomically resolved topography can be obtained when the tip is under a special condition. Figure 5(d) and 5(e) are two topographic images at the same area, with Fig. 5(d) showing the atomically resolved surface, on which the top S atoms can be discerned. The brightest atoms in each SD are the three nearest neighboring S atoms of the central Ta, leading to the triangle SDs in Fig. 5(e). The dashed triangles in Fig. 5(d) and 5(e) directly illustrate that the three-petal feature of the defect corresponds to the sites of next nearest S atoms of the central Ta atom. In Fig. 5(d), the black hole within the defect area indicates that the defect is possibly a missing central Ta, with both UHB and LHB suppressed in the defect spectrum. The origin of the raised peak below LHB is still an open question at current status. Then this special type of point defect can help to determine the atomic lattice arrangement as shown in Fig. 5(f).

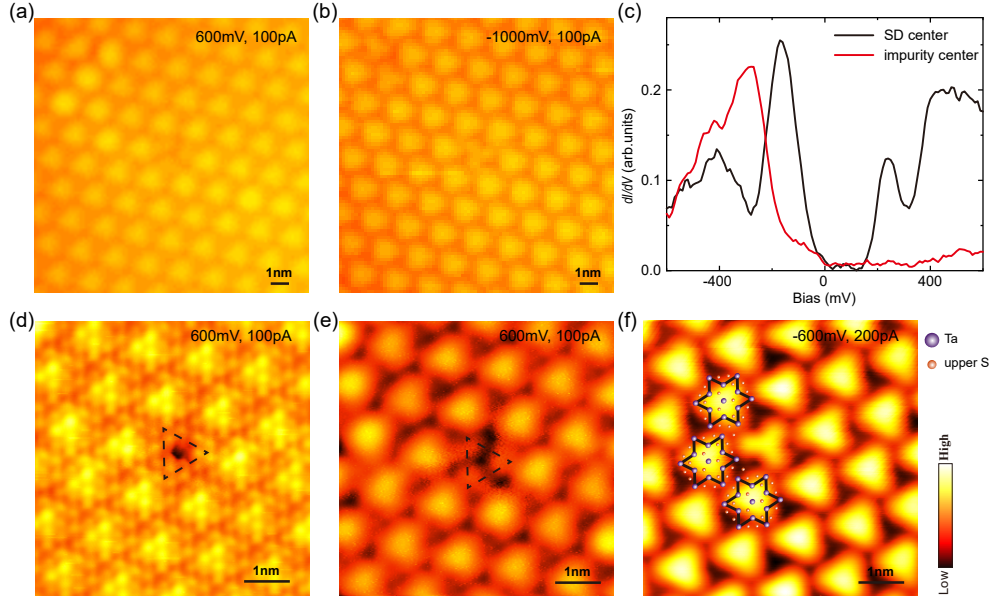


FIG. 5. Details of the three-petal shaped defect. (a), (b) Topographies including the same defect under positive and negative bias voltages. The tunneling condition is $V_b = -600$ mV and $I = 100$ pA in (a), and $V_b = -1$ V and $I = 100$ pA in (b). (c) The red and black curves show the dI/dV spectra measured at the center of one defect and a normal SD, respectively. (d) An atomically resolved three-petal shaped defect under the tunneling condition of $V_b = 600$ mV and $I = 200$ pA. (e) Topography at the same area as in (d). The dashed triangles in (d) and (e) indicate that three petals of the defect are at the sites of three next nearest S atoms. (f) Another topography with a three-petal shaped defect ($V_b = -600$ mV, $I = 200$ pA), with the structure of SD cluster superimposed.

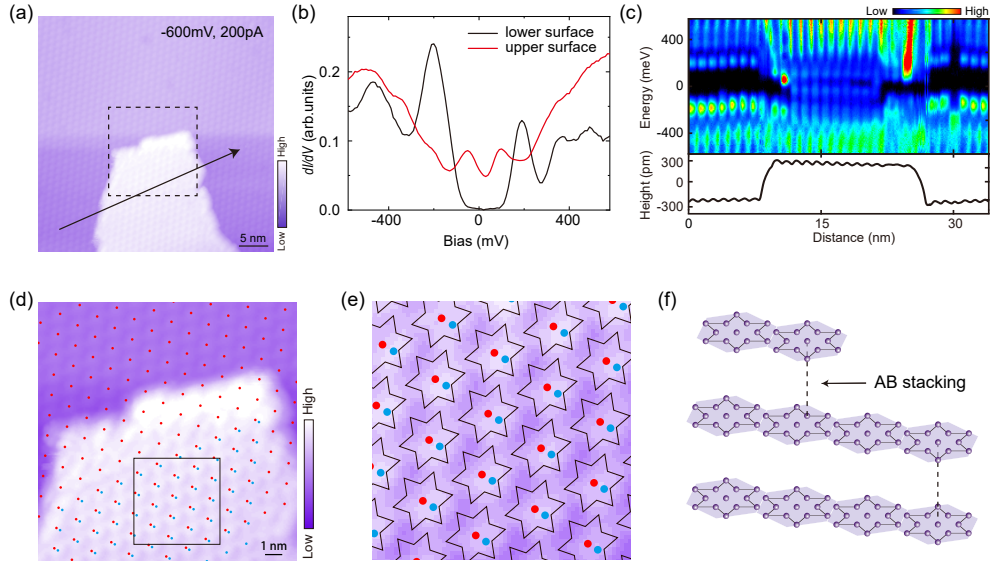


FIG. 6. AB-type stacking single-step area with a top metallic spectrum. (a) The STM topography of a special single-step area. (b) The red and black curves show the dI/dV spectra on the upper and lower terraces, respectively. The spectrum on the lower terrace is also the typical insulating spectrum, and on the upper terrace is a metallic spectrum. (c) A series of dI/dV spectra measured along the black arrowed line in (a), with the height profile displayed in the lower panel. (d) The determination of SD super-lattices for the area in the black dashed frame in (a). The red dots label SD centers in the lower layer, and the blue dots label SD centers in the upper layer. (e) The enlargement of the black box in (d). The SD centers in the upper layer are aligned with the SD inner-corner sites in the lower layer. (f) A schematic diagram of the AB-stacking order.

Appendix B: AB-stacking single-step area with a top metallic spectrum

Figure 6(a) shows the topography of an occasional example with a special stacking order. The corresponding dI/dV spectra measured on the lower and upper terraces are displayed in Fig. 6(b). The spectrum on the lower terrace is a large-gap insulating spectrum. The spectrum on the upper terrace exhibits a V-shape feature near the Fermi level, with the zero-bias conductance strongly enhanced, called a metallic spectrum in our paper. From the linecut map measured along the arrowed line [Fig. 6(c)], we observe that the coherent peaks of metallic spectrum are evident at the SD centers and orig-

inate from the Hubbard bands of central Ta orbital [28]. The SD centers in the upper and lower layers are similarly determined as in the main text. A SD array is obtained for the lower layer, as shown by the red dots in Fig. 6(d). The blue dots represent a shifted SD array compatible with the SD lattice in the upper layer [Fig. 6(d)]. In Fig. 6(e), both the SD centers and the SD arrangement in the lower layer are superimposed on the enlarged topography. We observe that the SD centers in the upper layer are aligned with the nearest Ta atoms in each SD in the lower layer. This stacking order is defined as the AB-stacking order [Fig. 6(f)]. From the result, we could see that the AB-stacking order plays a strongest perturbation to the upper-layer electronic state.

-
- [1] N. F. Mott, Metal-Insulator Transition, *Rev. Mod. Phys.* **40**, 677-683 (1968).
- [2] M. Imada, A. Fujimori, and Y. Tokura, Metal-Insulator Transitions, *Rev. Mod. Phys.* **70**, 1039 (1998).
- [3] P. A. Lee, N. Nagaosa, and X. G. Wen, Doping a Mott Insulator: Physics of High Temperature Superconductivity, *Rev. Mod. Phys.* **78**, 17-85 (2006).
- [4] D. Belitz and T. R. Kirkpatrick, The Anderson-Mott Transition, *Rev. Mod. Phys.* **66**, 261-380 (1994).
- [5] R. Manzke, T. Buslaps, B. Pfalzgraf, M. Skibowski, and O. Anderson, On the Phase Transitions in $1T$ -TaS₂, *Europhys. Lett.* **8**, 195-200 (1989).
- [6] P. Fazekas and E. Tosatti, Charge Carrier Localization in Pure and Doped $1T$ -TaS₂, *Phys. B + C* **99**, 183-187 (1980).
- [7] P. Fazekas and E. Tosatti, Electrical, Structural and Magnetic Properties of Pure and Doped $1T$ -TaS₂, *Phil. Mag. B* **39**, 229-244 (1979).
- [8] J. J. Kim, W. Yamaguchi, T. Hasegawa, and K. Kitazawa, Observation of Mott Localization Gap Using Low Temperature Scanning Tunneling Spectroscopy in Commensurate $1T$ -TaS₂, *Phys. Rev. Lett.* **73**, 2103 (1994).
- [9] F. Zwick, H. Berger, I. Vobornik, G. Margaritondo, L. Forró, C. Beeli, M. Onellion, G. Panaccione, A. Taleb-Ibrahimi, and M. Grioni Spectral Consequences of Broken Phase Coherence in $1T$ -TaS₂, *Phys. Rev. Lett.* **81**, 1058 (1998).
- [10] B. Sipos, A. F. Kusmartseva, A. Akrap, H. Berger, L. Forró, and E. Tutiš, From Mott State to Superconductivity in $1T$ -TaS₂, *Nat. mater.* **7**, 960-965 (2008).
- [11] Y. Liu, R. Ang, W. J. Lu, W. H. Song, L. J. Li, and Y. P. Sun, Superconductivity Induced by Se-Doping in Layered Charge-Density-Wave System $1T$ -TaS_{2-x}Se_x, *Appl. Phys. Lett.* **102**, 192602 (2013).
- [12] R. Ang, Y. Miyata, E. Ieki, K. Nakayama, T. Sato, Y. Liu, W. J. Lu, Y. P. Sun, and T. Takahashi, Superconductivity and Bandwidth-Controlled Mott Metal-Insulator Transition in $1T$ -TaS_{2-x}Se_x, *Phys. Rev. B* **88**, 115145 (2013).
- [13] K. T. Law and P. A. Lee, $1T$ -TaS₂ as a Quantum Spin Liquid, *Proc. Natl. Acad. Sci. USA* **114**, 6996-7000 (2017).
- [14] H. Murayama, Y. Sato, T. Taniguchi, R. Kurihara, X. Z. Xing, W. Huang, S. Kasahara, Y. Kasahara, I. Kimchi, M. Yoshida, Y. Iwasa, Y. Mizukami, T. Shibauchi, M. Konczykowski, and Y. Matsuda, Effect of Quenched Disorder on the Quantum Spin Liquid State of the Triangular-Lattice Antiferromagnet $1T$ -TaS₂, *Phys. Rev. Research* **2**, 013099 (2020).
- [15] M. Klanjšek, A. Zorko, R. Žitko, J. Mravlje, Z. Jagličič, P. K. Biswas, P. Prelovšek, D. Mihailovic, and D. Arčon, A High-Temperature Quantum Spin Liquid with Polaron Spins, *Nat. Phys.* **13**, 1130-1134 (2017).
- [16] P. Darancet, A. J. Millis, and C. A. Marianetti, Three-Dimensional Metallic and Two-Dimensional Insulating Behavior in Octahedral Tantalum Dichalcogenides, *Phys. Rev. B* **90**, 045134 (2014).
- [17] M. T. Suzuki and H. Harima, Electronic Band Structure of $1T$ -TaS₂ in CDW Phase, *J. Magn. Magn. Mater.* **E653**, 272-276 (2004).
- [18] F. J. Di Salvo and J. E. Graebner, The Low Temperature Electrical Properties of $1T$ -TaS₂, *Solid State Commun.* **23**, 825-828 (1977).
- [19] T. Ritschel, J. Trinckauf, K. Koepf, B. Büchner, M. v. Zimmermann, H. Berger, Y. I. Joe, P. Abbamonte and J. Geck, Orbital Textures and Charge Density Waves in Transition Metal Dichalcogenides, *Nat. Phys.* **11**, 328-331 (2015).
- [20] T. Ritschel, H. Berger, and J. Geck, Stacking-Driven Gap Formation in Layered $1T$ -TaS₂, *Phys. Rev. B* **98**, 195134 (2018).
- [21] S. H. Lee, J. S. Goh, and D. Cho, Origin of the Insulating Phase and First-Order Metal-Insulator Transition in $1T$ -TaS₂, *Phys. Rev. Lett.* **122**, 106404 (2019).
- [22] C. J. Butler, M. Yoshida, T. Hanaguri, and Y. Iwasa, Mottness Versus Unit-Cell Doubling as the Driver of the Insulating State in $1T$ -TaS₂, *Nat. Commun.* **11**, 2477 (2020).
- [23] C. J. Butler, M. Yoshida, T. Hanaguri, and Y. Iwasa, Doubloonlike Excitations and Their Phononic Coupling in a Mott Charge-Density-Wave System, *Phys. Rev. X* **11**, 011059 (2021).
- [24] J. Lee, K.-H. Jin, H.W. Yeom, Distinguishing a Mott Insulator from a Trivial Insulator with Atomic Adsorbates, *Phys. Rev. Lett.* **126**, 196405 (2021).
- [25] Y.D. Wang, W.L. Yao, Z.M. Xin, T.T. Han, Z.G. Wang, L. Chen, C. Cai, Y. Li, and Y. Zhang, Band Insulator to Mott Insulator Transition in $1T$ -TaS₂, *Nat. Commun.*

- 11**, 4215 (2020).
- [26] Q. Stahl, M. Kusch, F. Heinsch, G. Garbarino, N. Kretzschmar, K. Hanff, K. Rossnagel, J. Geck, and T. Ritschel, Collapse of Layer Dimerization in the Photo-Induced Hidden State of $1T$ -TaS₂, *Nat. Commun.* **11**, 1247 (2020).
- [27] L. J. Li, W. J. Lu, X. D. Zhu, L. S. Ling, Z. Qu, and Y. P. Sun, Fe-Doping-Induced Superconductivity in the Charge-Density-Wave System $1T$ -TaS₂, *Europhys. Lett.* **97**, 67005 (2012).
- [28] S. Qiao, X. T. Li, N. Z. Wang, W. Ruan, C. Ye, P. Cai, Z. Q. Hao, H. Yao, X. H. Chen, J. Wu, Y. Y. Wang, and Z. Liu, Mottness Collapse in $1T$ -TaS_{2-x}Se_x Transition-Metal Dichalcogenide: an Interplay Between Localized and Itinerant Orbitals, *Phys. Rev. X* **7**, 041054 (2017).
- [29] K. L. Bu, W. H. Zhang, Y. Fei, Z. X. Wu, Y. Zheng, J. J. Gao, X. Luo, Y. P. Sun, and Y. Yin, Possible Strain Induced Mott Gap Collapse in $1T$ -TaS₂, *Commun. Phys.* **2**, 146 (2019).
- [30] E. Lahoud, O. N. Meetei, K. B. Chaska, A. Kanigel, and N. Trivedi, Emergence of a Novel Pseudogap Metallic State in a Disordered 2D Mott Insulator, *Phys. Rev. Lett.* **112**, 206402 (2014).
- [31] Y. J. Yu, F. Y. Yang, X. F. Lu, Y. J. Yan, Y. H. Cho, L. G. Ma, X. H. Niu, S. Kim, Y. W. Son, D. L. Feng, S. Y. Li, S. W. Cheong, X. H. Chen, and Y. B. Zhang, Gate-Tunable Phase Transitions in Thin Flakes of $1T$ -TaS₂, *Nat. Nanotechnol.* **10**, 270-276 (2015).
- [32] H. C. Lin, W. T. Huang, K. Zhao, S. Qiao, Z. Liu, J. Wu, X. Chen, and S. H. Ji, Scanning Tunneling Spectroscopic Study of Monolayer $1T$ -TaS₂ and $1T$ -TaSe₂, *Nano Res.* **13**, 133-137 (2020).
- [33] Y. Chen, W. Ruan, M. Wu, S. J. Tang, H. Ryu, H. Z. Tsai, R. Lee, S. Kahn, F. Liou, C. H. Jia, O. R. Albertini, H. Y. Xiong, T. Jia, Z. Liu, J. A. Sobota, A. Y. Liu, J. E. Moore, Z. X. Shen, S. G. Louie, S. K. Mo, and M. F. Crommie, Strong Correlations and Orbital Texture in Single-Layer $1T$ -TaSe₂, *Nat. Phys.* **16**, 218-224 (2020).
- [34] L. G. Ma, C. Ye, Y. J. Yu, X. F. Lu, X. H. Niu, S. Kim, D. L. Feng, D. Tománek, Y. W. Son, X. H. Chen, and Y. B. Zhang, A Metallic Mosaic Phase and the Origin of Mott-Insulating State in $1T$ -TaS₂, *Nat. Commun.* **7**, 10956 (2016).
- [35] D. B. Shin, T. -D. Nicolas, J. Zhang, M. S. Okyay, A. Rubio, and N. Park, Identification of the Mott Insulating Charge Density Wave State in $1T$ -TaS₂, *Phys. Rev. Lett.* **126**, 196406 (2021).